Modeling and Compensation of Asymmetric Hysteresis Nonlinearity for Piezoceramic Actuators With a Modified Prandtl–Ishlinskii Model

Guo-Ying Gu, *Member, IEEE*, Li-Min Zhu, *Member, IEEE*, and Chun-Yi Su, *Senior Member, IEEE*

***Abstract*—This paper presents a modified Prandtl–Ishlinskii (P-I) (MPI) model for the asymmetric hysteresis description and compensation of piezoelectric actuators. Considering the fact that the classical P-I (CPI) model is only efficient for the symmetric hysteresis description, the MPI model is proposed to describe the asymmetric hysteresis nonlinearity of piezoceramic actuators (PCAs). Different from the commonly used approach for the development of asymmetric P-I models by replacing the classical play operator with complex nonlinear operators, the proposed MPI model still utilizes the classical play operator as the elementary operator, while a generalized input function is introduced to replace the linear input function in the CPI model. By this way, the developed MPI model has a relative simple mathematic format with fewer parameters to characterize the asymmetric hysteresis behavior of PCAs. The benefit for the developed MPI model also lies in the fact that an analytic inverse model of the CPI model can be directly applied for the inverse compensation of the asymmetric hysteresis nonlinearity represented by the developed MPI model in real-time applications. To validate the developed MPI model and the inverse hysteresis compensator, simulation, and experimental results on a piezoceramic actuated platform are presented.**

***Index Terms*—Asymmetric hysteresis nonlinearity, inverse hysteresis compensation, modified Prandtl–Ishlinskii (P-I) (MPI) model, piezoceramic actuator (PCA).**

I. Introduction

PIEZOELECTRICITY is the electromechanical phenomenon of strong coupling between the electrical properties and mechanical properties of some piezoelectric materials. Mechanical stresses in the piezoelectric materials produce measurable electric charge, which is referred to as the direct piezoelectric effect. Conversely, mechanical strains are generated in response to an applied electric field, and this is called the converse piezoelectric effect. In general, the direct effect is the basis for sensing applications, and the converse effect is used for precision actuation and manipulation in control applications. Due to the excellent advantages of large output force, high bandwidth, and fast response time, piezoceramic actuators (PCAs) made of piezoelectric materials have been widely used for a long time in nanopositioning applications [1]–[4] such as scanning probe microscopes, nanoimprint equipment, and micro-/nanomanipulations. However, piezoceramic materials suffer from the strong hysteresis effect. It can significantly degrade the performance of the PCAs which leads, in the best case, to reduce the motion accuracy and, in the worst case, to destabilize the control system [5]–[9].

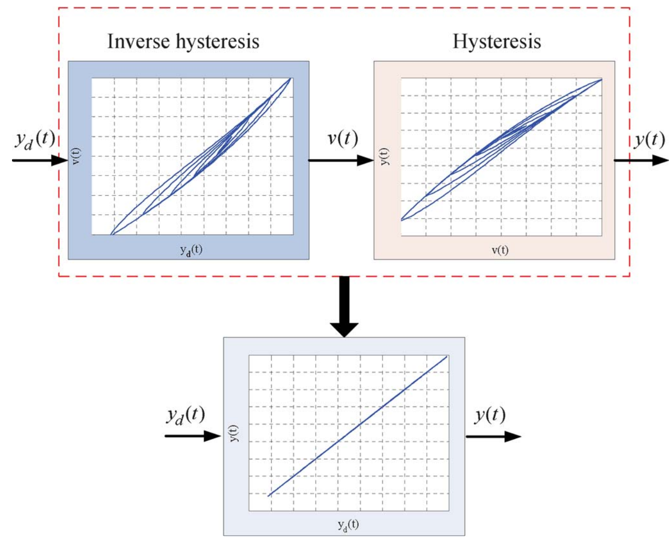

Fig. 1. Schematic illustration of the feedforward control technique for hysteresis compensation.

To address such a challenge, many efforts have been made to compensate for the hysteresis nonlinearity in PCAs. Feedforward control is the most common used approach [10], [11]. The main idea of the feedforward control approach is to develop a mathematical model that describes the complex hysteresis nonlinearity and, then, to implement a feedforward controller based on the inverse hysteresis model to linearize the actuator response, which can be schematically shown in Fig. 1. It refers, in particular, to the utilization of a hysteresis model accurately describing the hysteresis nonlinearity. As a matter of fact, there are two kinds of hysteresis modeling approaches, which are the physics-based hysteresis models and phenomenological

Manuscript received November 21, 2012; revised January 31, 2013; accepted March 16, 2013. Date of publication April 5, 2013; date of current version August 23, 2013. This work was supported in part by the National Natural Science Foundation of China under Grant 91023047, in part by the Science and Technology Commission of Shanghai Municipality under Grant 11520701500, in part by the Shu Guang Project supported by the Shanghai Municipal Education Commission under Grant 10SG17, and in part by the China Postdoctoral Science Foundation under Grant 2013M530193.

G.-Y. Gu and L.-M. Zhu are with the State Key Laboratory of Mechanical System and Vibration, Shanghai Jiao Tong University, Shanghai 200240, China (e-mail: guguoying@sjtu.edu.cn; zhulm@sjtu.edu.cn).

C.-Y. Su is with the College of Automation Science and Engineering, South China University of Technology, Guangzhou 510641, China, on leave from Concordia University, Montreal, QC H3G 1M8, Canada (e-mail: cysu@alcor.concordia.ca).

Color versions of one or more of the figures in this paper are available online at http://ieeexplore.ieee.org.

Digital Object Identifier 10.1109/TIE.2013.2257153

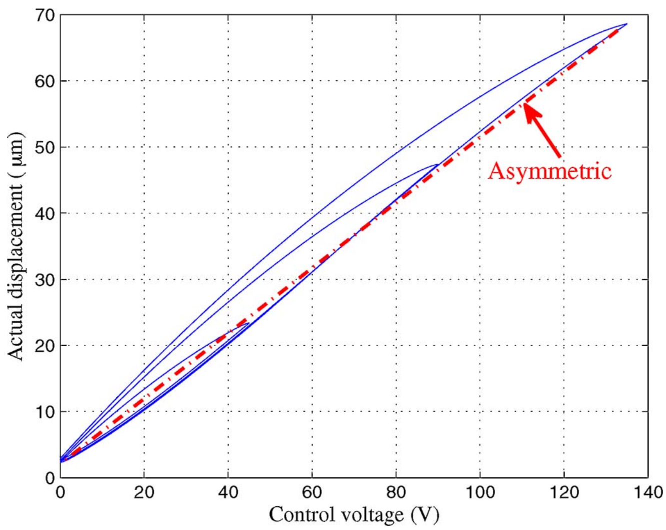

Fig. 2. Asymmetric hysteresis loops of a PCA.

hysteresis models. The physics-based models [12], [13] are derived on the basis of a physical measure, such as energy, displacement, or stress–strain relationship, while phenomenological hysteresis models [14]–[16] are constructed from the experimental data without considering the physical property of the actuator. Readers may refer to [17]–[21] and the references therein for reviewing recent studies on hysteresis modeling. A popular phenomenological hysteresis model adopted for the hysteresis modeling and compensation of PCAs is the Preisach model [6], [22], [23]. The main limitation is that the Preisach model is not analytically invertible. Thus, numerical methods are generally adopted to obtain approximate inversions of the Preisach model [24]–[27]. As a subclass of the Preisach model, the Prandtl–Ishlinskii (P-I) model [28] is an alternative effective method to describe the hysteresis nonlinearity by a single threshold variable together with a density function. Compared with the Preisach model, the main advantages of the P-I model are the reduced modeling complexity and the analytical inverse for the P-I model, thus making it more efficient for real-time applications [29]–[33]. However, the classical P-I (CPI) model is limited to the symmetric hysteresis description. It cannot be utilized when an asymmetry exists in the hysteresis loops, such as those observed in the input–output relations of the PCAs depicted in Fig. 2. In an attempt to overcome this drawback of the CPI model, researchers have proposed several variations of P-I models for characterizing the asymmetric hysteresis loops. Kuhnen [34] in the first time proposed dead-zone operators cascaded with the classical play operator to describe the asymmetric hysteresis nonlinearity. Instead of using the symmetric play operator, Dong and Tan [35] utilized an asymmetric backlash operator as the elementary operator for asymmetric hysteresis modeling. As another choice in [36], two asymmetric operators were utilized for the ascending and descending branches of hysteresis loops, respectively. Using two nonlinear envelope function-based play operators, a generalized P-I model [18] was proposed to describe a more general class of hysteresis loops which are observed in magnetostrictive actuators or shape memory alloy actuators. These reported works [18], [34]–[36] for P-I models generally replace the classical play operator by modified or nonlinear play operators with more complex formats under different conditions, and experimental results are applied to verify the effectiveness of the asymmetric hysteresis representation and compensation.

In this paper, a novel modified P-I (MPI) model that originates from the CPI model is developed to describe the asymmetric hysteresis nonlinearity of PCAs. In contrast, to change the formulation of the play operators as reported in [18] and [34]–[36], the classical play operator is still utilized to serve as the elementary operator in the developed MPI model, while a generalized input function is introduced to replace the linear input function in the CPI model. Thus, the hysteresis shapes can be determined by not only the weighted play operators but also the generalized input function. The main advantages of the developed MPI model lie in the following facts: 1) Rather than using the nonlinear dead-zone operators or the modified or nonlinear play operators, the classical play operator is still utilized in the MPI model to serve as the elementary operator; 2) the MPI model has a relative simple mathematic format with fewer parameters to describe the asymmetric hysteresis behavior of PCAs; and 3) an analytic inverse of the MPI model can be directly derived from the inverse of the CPI model for the purpose of the feedforward hysteresis compensation in real-time applications. To validate the developed MPI model and the inverse hysteresis compensator, simulation and experimental results on a piezoceramic actuated platform are presented.

The remainder of this paper is organized as follows. Section II introduces the MPI model and its analytical inverse. Section III presents the simulation verification of properties of the developed MPI model. Finally, the experimental validation of the developed MPI model and its inverse hysteresis compensator on a piezoceramic actuated platform is presented in Section IV, and Section V concludes this paper.

II. MPI Model

Before introducing the proposed MPI model, the CPI model is first reviewed in brief.

A. CPI Model

The CPI model [28] is a famous operator-based phenomenological model, which utilizes the weighted play operators and a linear input function to describe the hysteresis nonlinearity. The play operator is the basic hysteresis operator with symmetric and rate-independent properties. The 1-D play operator can be considered as a piston with a plunger of length $2r$. The output w is the position of the center of the piston, and the input is the plunger position v. According to the definition in [28], the play operator $w(t) = F_r[v](t)$ with a threshold r for any piecewise monotone input function $v(t) \in C_m[0, t_E]$ is expressed as

$$\begin{aligned} w(0) &= F_r[v](0) = f_r\left(v(0), 0\right) \\ w(t) &= F_r[v](t) = f_r\left(v(t), w(t_i)\right) \end{aligned} \quad (1)$$

for $t_i < t \leq t_{i+1}, 0 \leq i \leq N-1$, with

$$f_r(v, w) = \max\left(v - r, \min(v + r, w)\right) \quad (2)$$

where $0 = t_0 < t_1 < \ldots < t_N = t_E$ is a partition of $[0, t_E]$ such that the function $v(t)$ is a monotone on each of the

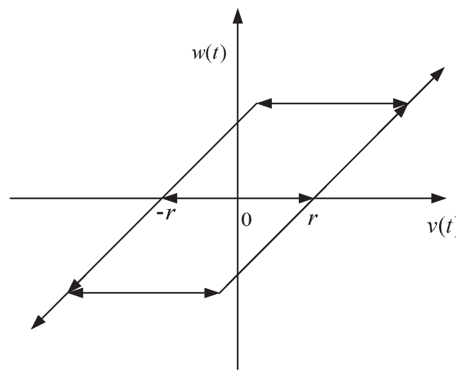

Fig. 3. Input–output relationships of the play operator (1).

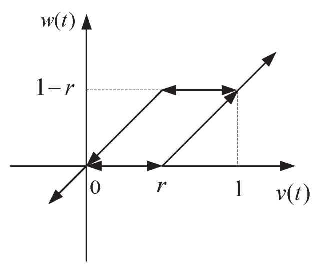

Fig. 4. Input–output relationships of the OSP operator (3).

subintervals $[t_i, t_{i+1}]$. The argument of the operator (1) is written in square brackets to indicate the functional dependence since it maps a function to another function. The play operator has the rate-independent property, i.e., the output of the play operator is only influenced by the current input value and the past extrema of input function $v(t)$ while the velocity of input variation between each extreme shall not affect the shape of the output. As an illustration, Fig. 3 shows the transfer characteristics of the play operator (1).

Consider the fact that the PCAs have the positive excitation nature. Rather than using the play operator in (2), a one-side play (OSP) operator is adopted in this work. The OSP operator $F_{or}[v](t)$ with a threshold $r \geq 0$ for any piecewise monotone input function $v(t) \in C_m[0, t_E]$ is defined as

$$\begin{aligned} w(0) &= F_{or}[v](0) = f_{or}\,(v(0), 0) \\ w(t) &= F_{or}[v](t) = f_{or}\,(v(t), w(t_i)) \end{aligned} \tag{3}$$

for $t_i < t \leq t_{i+1}, 0 \leq i \leq N-1$, with

$$f_{or}(v, w) = \max\left(v - r, \min(v, w)\right) \tag{4}$$

for $0 = t_0 < t_1 < \ldots < t_N = t_E$. For comparison, Fig. 4 shows the transfer characteristics of the OSP operator (3).

Remark: It should be noted that the advantage for choosing the OSP operator lies in that, when describing the hysteresis nonlinearity, we avoid to calculate the expression of $v + r$ at each threshold r. The following simulation and experimental results will further demonstrate that, with the OSP operator, the proposed MPI model is good enough for the asymmetric hysteresis description of PCAs.

The CPI model utilizes the aforementioned OSP operator $F_{or}[v](t)$ to describe the relationship between the output y_c and the input v as [28], [29]

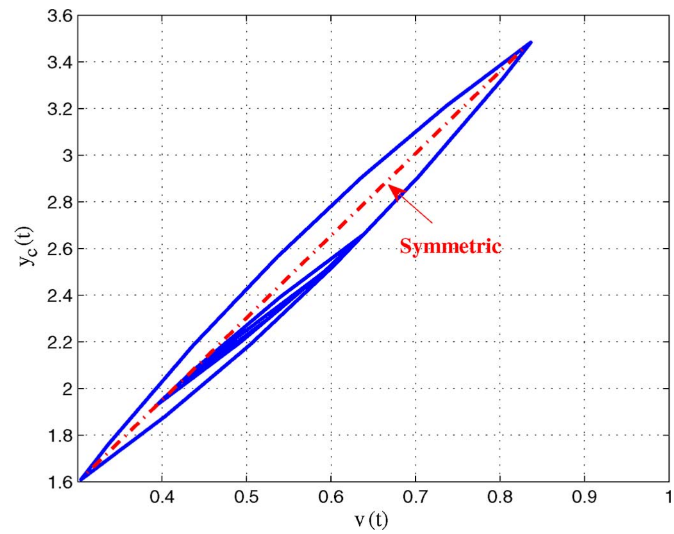

Fig. 5. Hysteresis loops generated by the CPI model (5).

$$y_c(t) = P[v](t) = p_0 v(t) + \int_0^R p(r) F_{or}[v](t)\, dr \tag{5}$$

where $p(r)$ is a density function that is generally calculated from the experimental data and p_0 is a positive constant. The density function $p(r)$ generally vanishes for large values of r, while the choice of $R = \infty$ as the upper limit of integration is widely used in the literature for the sake of convenience [18], [30].

Remark: It should be noted that there is no general criterion for the selection of the density function $p(r)$. Generally, it is completely selected by the designer. Once the structure of the density function $p(r)$ is fixed, the parameters involved in the density function shall be determined by identification from experimental data in order to best reflect the shapes of the hysteresis exhibited in PCAs.

From (5), the CPI model is defined in terms of an integral of the OSP operator $F_{or}[v](t)$ with a density function $p(r)$ and an linear input function $p_0 v(t)$. According to the symmetric properties of the play operator and the linear function, the CPI model can only be used to characterize the symmetric hysteresis nonlinearity. As an illustration, Fig. 5 shows the hysteresis loops generated by the CPI model (5) with $p_0 = 2.42$, $p(r) = 5e^{-0.505(r-1)^2}$, $r \in [0, 1]$, and the input $v(t) = 0.5 + 0.5\sin(3t)/(1+t)$. It can be observed that the generated hysteresis loops in Fig. 5 are symmetric. However, the real hysteresis nonlinearity of the PCA exhibits the asymmetric shape as shown in Fig. 2. Therefore, the CPI model yields considerable errors for the description of the asymmetric hysteresis nonlinearity. One of the motivations of this work is to find an effective model that can accurately represent the asymmetric hysteresis nonlinearity of PCAs.

B. MPI Model

Considering the fact that the CPI model is developed for the symmetric hysteresis description, a novel MPI model is proposed in this work to characterize the asymmetric hysteresis behavior of PCAs. It is worthy of mentioning that, although several models [18], [34]–[36] have been reported to overcome the drawback of the CPI model that can only describe the symmetric hysteresis, the developed MPI model in this work is different from them. Analyzing the structure of the CPI model (5), it consists of two parts. The first part is a linear input function $p_0 v(t)$, and the second one is the integral of the OSP operator $F_{or}[v](t)$ with a density function $p(r)$. According to the two-part structure of the CPI model, the previous reported models in [18] and [34]–[36] focus on the modification of play operators in the second part with more complex formats under different conditions. In contrast, to change the play operator, we develop a model to modify the first part of the CPI model with a generalized input function, keeping the second part the same with the CPI model. One reason for this alternative choice is motivated by the fact that the classical play operator is still utilized to serve as the elementary operator. In such a way, the developed MPI model has a relative simple mathematic format with fewer parameters to characterize the asymmetric hysteresis behavior of PCAs. Another advantage is that an analytic inverse of the MPI model can be directly derived from the inverse of the CPI model for the real-time feedforward hysteresis compensation, which will be shown in the following development.

In this paper, the proposed MPI model is formulated as

$$y_g(t) = P_g[v](t) = g\left(v(t)\right) + \int_0^R p(r) F_{or}[v](t)\, dr \qquad (6)$$

where $g(v(t))$ is a generalized odd input function with the memoryless and locally Lipschitz continuous properties and $p(r)$ and $F_{or}[v](t)$ are defined the same as the ones in the CPI model (5). Since the polynomial function [37], [38] is generally recognized as an effective choice to describe the hysteresis loops, a third-degree polynomial input function $g(v(t)) = a_1 v^3(t) + a_2 v(t)$ with two coefficients a_1 and a_2 is utilized in the developed MPI on the asymmetric hysteresis characterization of PCAs.

Comparing (6) with (5), the difference between the MPI model and the CPI model lies on the selection of the input function $g(v(t))$. If $g(v(t))$ is selected as $g(v(t)) = p_0 v(t)$, the MPI model can be directly reduced to the classical one. Therefore, the CPI model can be considered as a special case of the MPI model. The benefit for choosing the generalized input function $g(v(t))$ (a third-degree input function in this work) is that the proposed MPI model can characterize the real hysteresis nonlinearity of the PCA with the asymmetric behavior. To elucidate this advantage of the MPI model, Fig. 6 shows the hysteresis loops generated by the MPI model (6) with $g(v(t)) = -v^3(t) + 2.42v(t)$. It is worthy of mentioning that the density function $p(r)$ and input $v(t)$ are chosen the same as the ones used in the CPI model that generates the hysteresis loops in Fig. 5. As a contrast, it is the polynomial input function $g(v(t))$ that makes the MPI model accommodate a more general class of hysteresis shapes with the asymmetric behavior.

Remarks:

1) Due to the rate-independent characteristic of the OSP operator and the generalized input function, the proposed MPI model is a rate-independent hysteresis model like the previous reported models in [18], [32], and [34]–[36], which can describe hysteresis loops that are invariant with respect to the frequency of the input.
2) It should be noted that the developed MPI model is formulated by (6), where the asymmetric part is generated by the selection of $g(v(t))$. A third-order polynomial is chosen due to the fact that it can present reasonable complicated shapes of the hysteresis, taking into consideration of the inverse calculations and number of parameters. Furthermore, the third-order polynomial [37], [38] is generally recognized as an effective choice to describe the hysteresis loops. Certainly, the selection of $g(v(t))$ is not unique, and other forms can also be chosen. For the development of this paper, a form has to be fixed, and we select a third-order polynomial due to the aforementioned reasons.

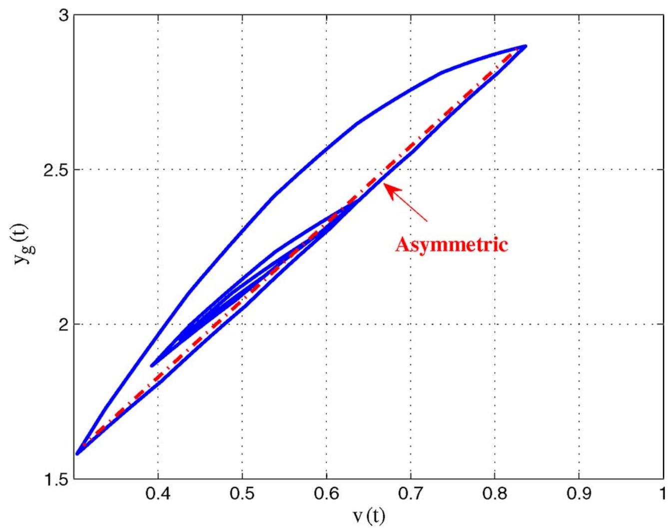

Fig. 6. Hysteresis loops generated by the MPI model (6).

C. Inverse MPI Model

The main idea of the inverse hysteresis compensation is to cancel the hysteresis nonlinearity by cascading the inverse hysteresis model with the real hysteresis as shown in Fig. 1. In the above section, the MPI model is developed based on the CPI model to describe the asymmetric hysteresis nonlinearity. In this section, we will show that the inverse of the CPI model can also be directly applied to the MPI case.

In order to conveniently implement the real-time inverse controller, the definition of the MPI model given in (6) can be approximated in the form of a finite number of the OSP operators as follows:

$$y_g(t) = P_g[v](t) = a_1 v^3(t) + a_2 v(t) + \sum_{i=1}^{n} b(r_i) F_{or_i}[v](t) \qquad (7)$$

where n is the number of the adopted play operators for modeling and $b(r_i) = p(r_i)(r_i - r_{i-1})$ is the weighted coefficient for the threshold r_i.

On the basis of the CPI model (5) and inspired by the work in [6], the MPI model (7) can be re-expressed as the following

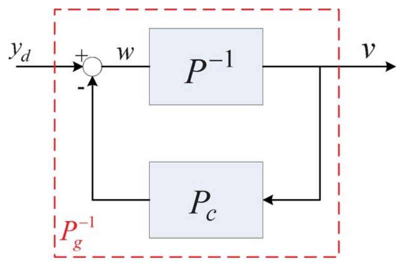

Fig. 7. Signal flow chart of the inverse compensator P_g^{-1}.

superposition:

$$y_g(t) = P_g[v](t) = P_c[v](t) + P[v](t) \tag{8}$$

where $P_c[v](t) = a_1 v^3(t)$ is a new model component.

The synthesis of efficient real-time control algorithms for the compensation of the asymmetric hysteresis nonlinearity represented by the MPI model is based on the implicit operator equation

$$v(t) = P^{-1}[w](t) \tag{9}$$

for the inverse compensator

$$v(t) = P_g^{-1}[y_g](t) \tag{10}$$

where $w = y_d - P_c[v]$, $y_d(t)$ is the desired displacement, and the inverse CPI hysteresis model [30]P^{-1} is used as a subsystem expressed as

$$P^{-1}[w](t) = \hat{a}_2 w(t) + \sum_{j=1}^{n} \hat{b}_j F_{\widehat{or_j}}[w](t) \tag{11}$$

with

$$\begin{aligned} \hat{r}_j &= a_2 r_j + \sum_{i=1}^{j-1} b_i (r_j - r_i) \\ \hat{a}_2 &= \frac{1}{a_2} \\ \hat{b}_j &= -\frac{b_j}{\left(a_2 + \sum_{i=1}^{j-1} b_i\right)\left(a_2 + \sum_{i=1}^{j} b_i\right)}. \end{aligned} \tag{12}$$

Fig. 7 shows the signal flow chart of the inverse compensator P_g^{-1} for the developed MPI model. By this way, the analytical inverse hysteresis model of CPI [30] can be directly applied for the asymmetric hysteresis compensation of PCAs described by the developed MPI model.

III. Verification of Wiping-Out and Congruency Properties by Simulation

The wiping-out and congruency properties are essential properties for the validity of the operator-based hysteresis models [15], [28]. In the following development, we will show by simulation that the proposed MPI model also fulfills these two properties.

A. Wiping-Out Property

The wiping-out property refers to the nonlocal memoryless behavior that the hysteresis output depends upon not only the current input but also the previous dominant input extrema. In other words, only the alternating series of the dominant input extrema are stored by the hysteresis model, and all other input extrema are wiping out. It can be shown that the developed MPI model possesses this property.

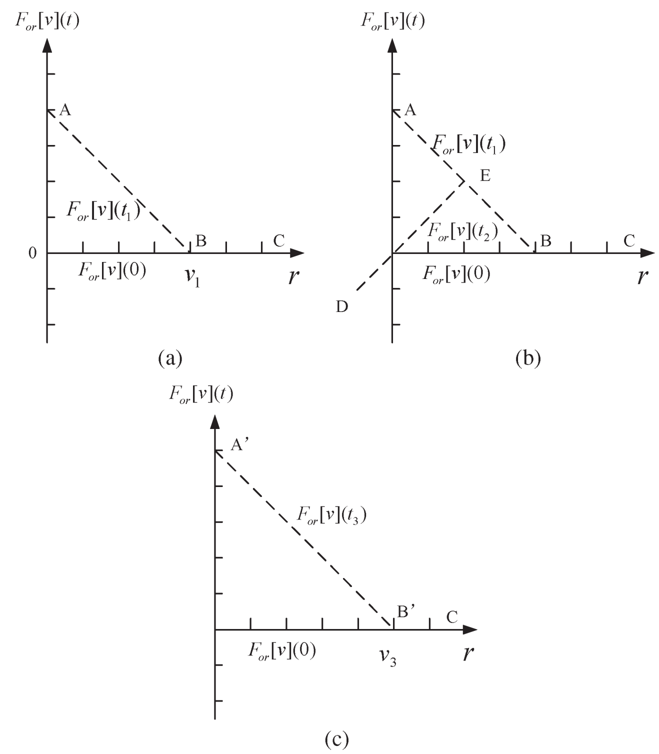

Fig. 8. Geometrical interpretation of the wiping-out property with the memory curve structure.

Inspired by the validation approach of the wiping-out property for the operator-based hysteresis models [15], [27], [28], [39], the wiping-out property of the proposed MPI model is asserted in a geometrical interpretation with the memory curve structure. To this end, we first demonstrate that the OSP operator possesses the wiping-out property. Suppose that an input function v satisfies $v_0 = 0$ at time t_0. At this time, we have $F_{or}[v](0) \equiv 0$ for $r \geq 0$. Next, suppose that the input function v is increased monotonically to a value v_1 at time t_1. By the definition of $F_{or}[v]$ in (3), $F_{or}[v](t_1) = \max(v_1 - r, 0)$ is the line segment ABC as shown in Fig. 8(a). If the input is then monotonically decreased from v_1 to v_2 at time t_2, $F_{or}[v](t_2) = \min(v_2, F_{or}[v](t_1))$ is the line segment $DEBC$ as shown in Fig. 8(b). Then, the input is monotonically increased from v_2 to v_3 at time t_3 satisfying $v_3 > v_1$, and $F_{or}[v](t_3) = \max(v_3 - r, F_{or}[v](t_2))$ is the line segment $A'B'C$ as shown in Fig. 8(c). Thus, the memory behavior at time t is completely described by the memory curve $F_{or}[v](t)$. It is evident that the dominant input extrema lower than v_3 have been wiping out. It can be concluded that the OSP operator possesses the wiping-out property. In addition, the wiping-out property follows the linear superposition [28], [39], and the introduced input function $g(v(t))$ is odd and memoryless. Therefore, the developed MPI model still fulfills the wiping-out property, which can be further illustrated by the following simulation example.

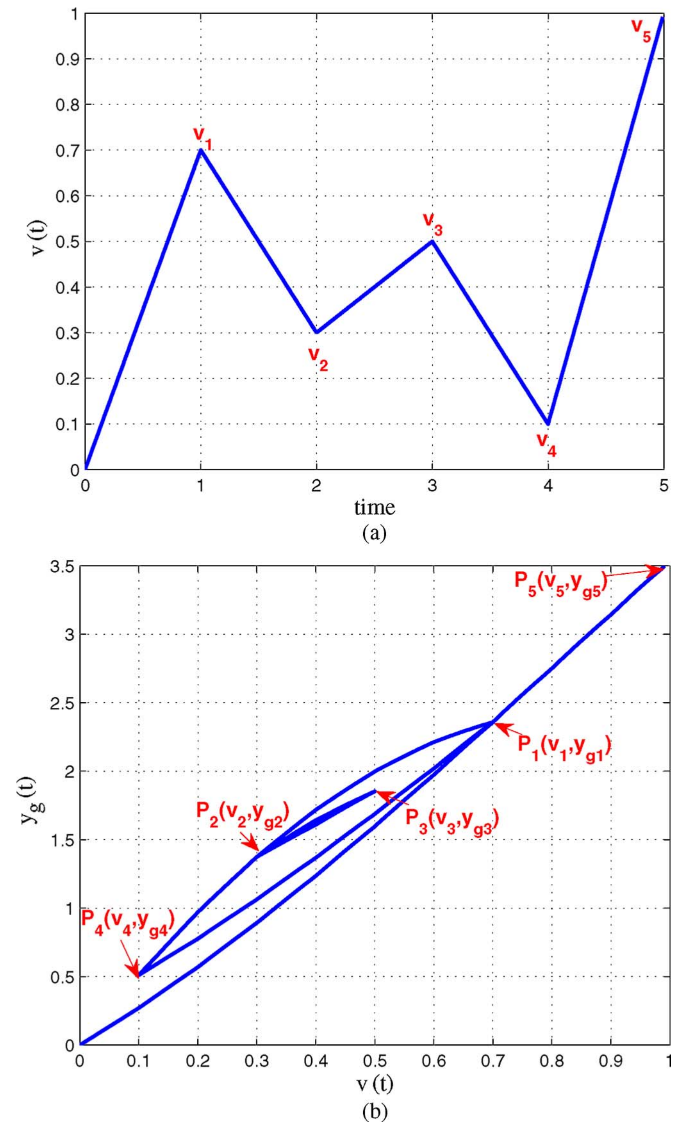

Fig. 9. Simulation of the wiping-out property. (a) Input voltage. (b) Hysteresis loops.

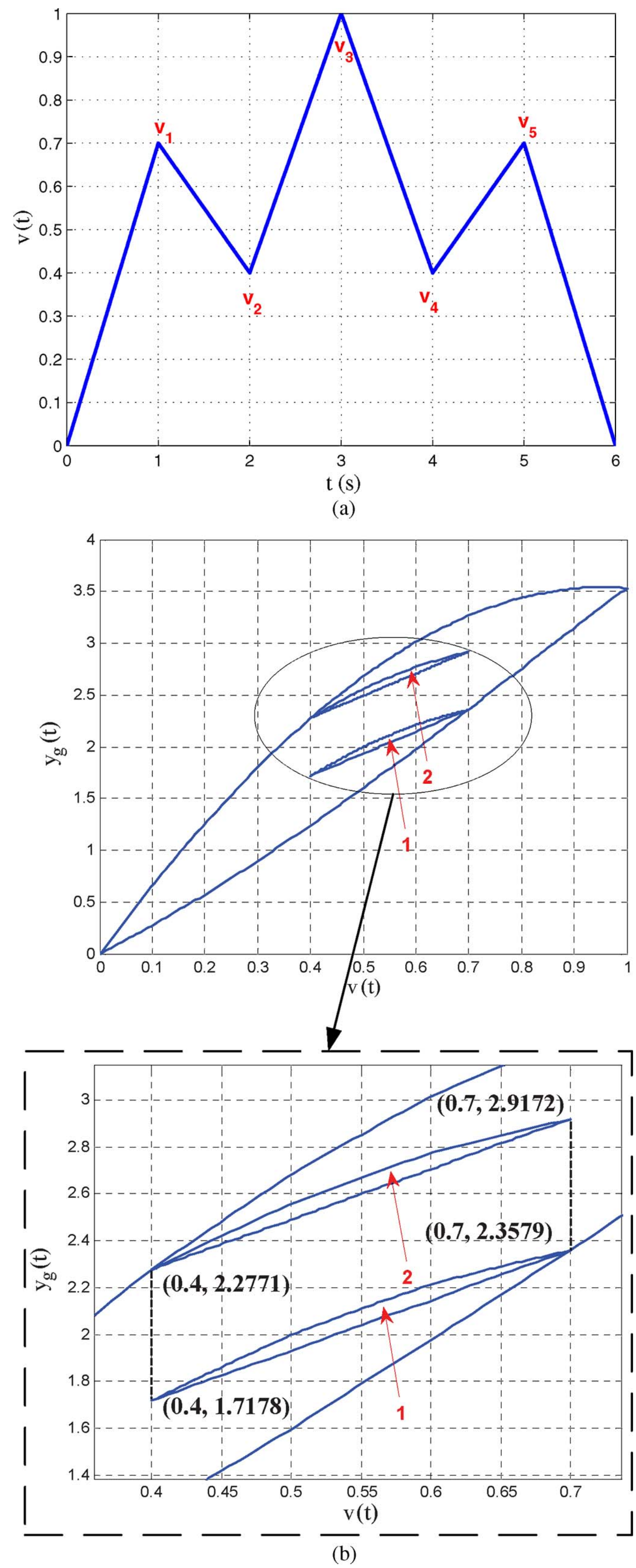

Fig. 10. Simulation of the congruency property. (a) Input voltage. (b) Hysteresis loops.

In Fig. 9(a), a special input function, having a given input string sequence of extrema $(0, v_1, v_2, v_3, v_4, v_5)$, is chosen in the simulation so as to verify the wiping-out property discussed earlier. When the input function and density function are respectively chosen as $g(v)(t) = -v^3(t) + 2.42v(t)$ and $p(r) = 5e^{-0.505(r-1)^2}$, Fig. 9(b) gives the generated hysteresis loops corresponding to the input history shown in Fig. 9(a). In the output–input plane of Fig. 9(b), $P_i = (v(t_i), y_g(t_i))$, $i = 0, 1, \ldots, 5$, represents the associated memories with the input string sequence $(0, v_1, v_2, v_3, v_4, v_5)$. In the beginning, the input $v(t)$ starts from its initial value of 0 and quickly reaches its first maximum value v_1. The process takes the trajectory from an initial point (0, 0) to memory point $P_1(v_1, y_{g1})$ following the $\overrightarrow{0P_1}$ curve of the hysteresis loops as shown in Fig. 9(b). After that, the input $v(t)$ decreases to its first minimum value v_2, and the corresponding output–input relationship switches into the $\overrightarrow{P_1P_2}$ curve. Subsequently, the input $v(t)$ increases to its second maximum value v_3. Correspondingly, the output–input trajectory of the hysteresis loops moves from point $P_2(v_2, y_{g2})$ to point $P_3(v_3, y_{g3})$. Since the second maximum value v_3 is lower than the first maximum one v_1, i.e., $v_3 < v_1$, the wiping-out phenomenon does not occur so far. Next, the input $v(t)$ decreases to the second minimum value v_4, and this

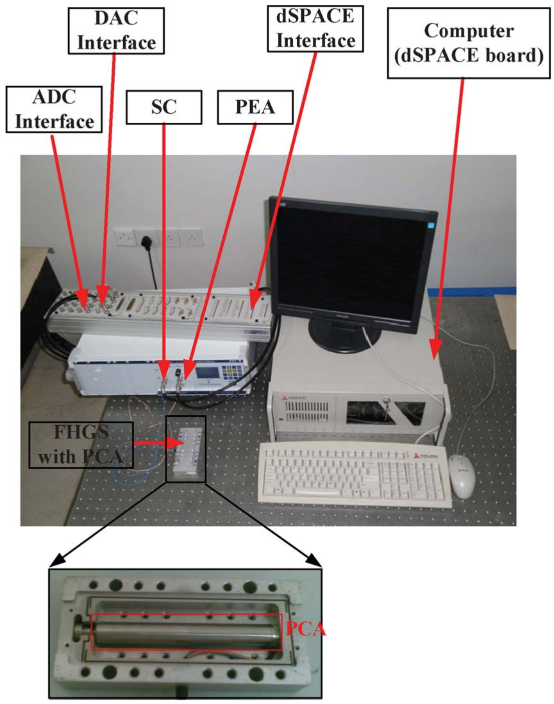

Fig. 11. Experimental platform.

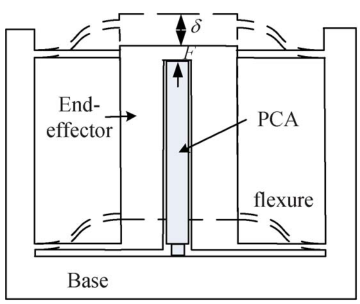

Fig. 12. Schematic structure of the PCA-actuated 1-D flexure mechanism.

process corresponds to the $\overrightarrow{P_3P_2P_4}$ curve. At this moment, the second minimum value v_4 is lower than the first minimum one v_2, i.e., $v_4 < v_2$. The memory $P_2(v_2, y_{g2})$ is wiped out by the memory $P_4(v_4, y_{g4})$. In the end, the input $v(t)$ continues to increase from v_4 to its third maximum value v_5. Since $v_5 > v_1 > v_3$, from Fig. 9(b), it can be observed that the memories $P_1(v_1, y_{g1})$ and $P_3(v_3, y_{g3})$ are both wiped out by the memory $P_5(v_5, y_{g5})$. During this period, the hysteresis curve switches to the $\overrightarrow{P_4P_1P_5}$ branch, and this process will not be affected by any past maximum values because all the memories about the past input maximum values have been completely wiped out. Using this example, we can see that the MPI model successfully fulfills the wiping-out property.

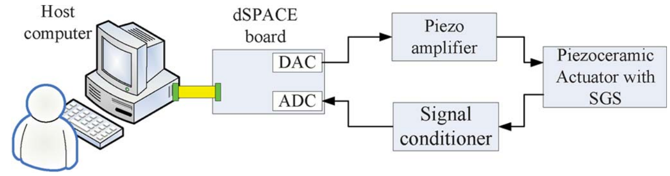

Fig. 13. Block diagram of the experimental platform.

TABLE I
IDENTIFIED PARAMETERS OF THE MPI MODEL

Number	r_i	b_i	a_i
1	0	0.2313	-0.1569
2	0.1	0.3059	0.4603
3	0.2	0.0155	
4	0.3	0.0752	
5	0.4	0.0683	
6	0.5	0.0252	
7	0.6	0.0035	
8	0.7	0.0094	
9	0.8	0.0264	
10	0.9	0.0032	

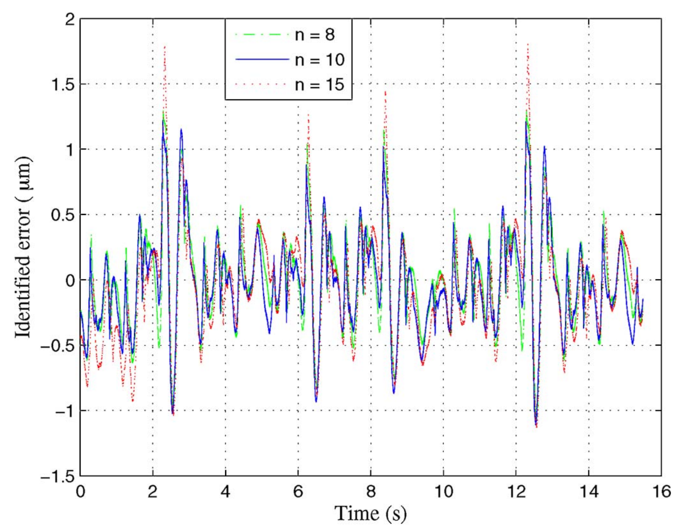

Fig. 14. Identification errors with different selections of n.

TABLE II
QUANTIFIED COMPARISON OF PARAMETERS IN DIFFERENT MODELS

Model	Parameters' number
Kuhnen [34] $n = 10, l = 4$	29
Dong [35] $n = 10$	50
Jiang [36] $n = 10$	51
Janaideh [18] $n = 10$	32
Proposed $n = 10$	22

B. Congruency Property

The congruency property means that two minor hysteresis loops corresponding to the the same input range are congruent. By adopting the memory curve [15], [27], [28], [39], it can be shown that the MPI model possesses the congruency property as well.

For example, the input $v(t)$ for validation is given in Fig. 10(a). In this case, the input string sequence of input maxima and minima is defined as $(0, v_1, v_2, v_3, v_4, v_5, 0)$, where $v_1 = v_5$ and $v_2 = v_4$. Thus, the input ranges $[v_2, v_1]$ and $[v_4, v_5]$ are the same. For the input voltage shown in Fig. 10(a), the associated hysteresis loops generated by the MPI model are given in Fig. 10(b). In Fig. 10(b), the lower minor hysteresis loop 1 is caused by the input wavering between the values v_2 and v_1 in the ascending process, and the upper minor hysteresis

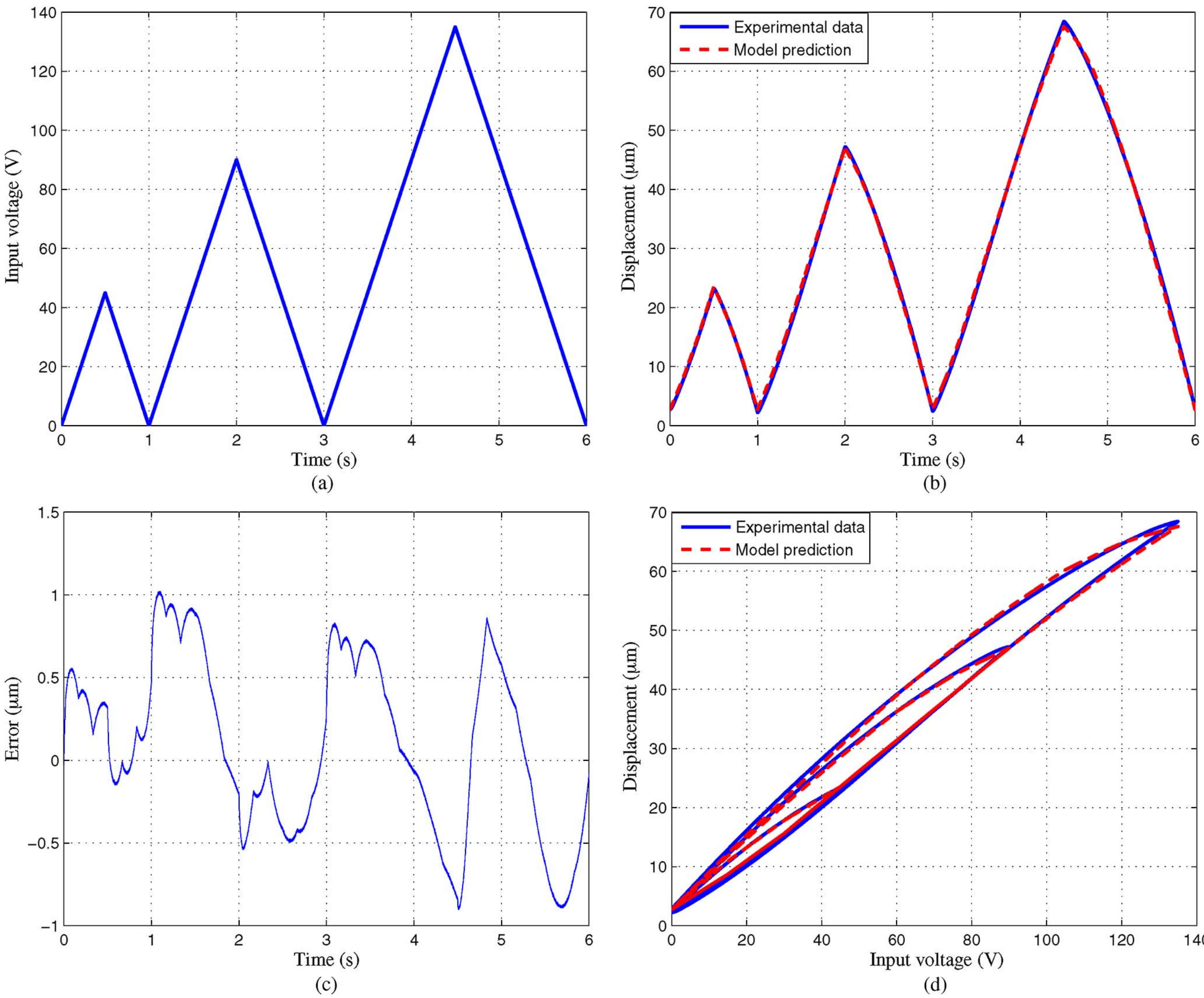

Fig. 15. Experimental verification of the MPI model with a simple input signal. (a) Input voltage. (b) Displacement. (c) Error. (d) Hysteresis loops.

loop 2 is led by the input wavering between the values v_4 and v_5 with the same range in the descending process. It can be observed that one of the two minor hysteresis loops can exactly overlap the other one if the loop 1 is shifted upside along the vertical direction by 0.5593 unit without rotation, which demonstrates that the two minor loops are congruent.

IV. Experimental Verification

In this section, an experimental platform with a piezoceramic actuator will be established, and experimental tests shall be conducted to verify the developed MPI model and the corresponding inverse hysteresis compensator for the PCA with the asymmetric hysteresis nonlinearity.

A. Experimental Setup

The experimental platform is shown in Fig. 11. It consists of a host computer, a dSPACE-DS1103 controller board, a PCA, a piezoelectric amplifier (PEA), a strain gauge position sensor, and a sensor signal conditioner (SC). The host computer provides a user interface for the dSPACE-DS1103 controller board. The dSPACE-DS1103 controller board equipped with 16-b digital-to-analog converters and 16-b analog-to-digital converters is adopted to generate control codes and obtain the displacement information. The PCA is a preloaded piezoceramic stack actuator (PSt 150/7/100 VS12 from Piezomechanik in Germany), which is used to drive the 1-D flexure hinge guiding stage (FHGS) with the nominal 75-μm displacement. Fig. 12 shows the schematic structure and work principle of the PCA-actuated 1-D flexure mechanism, where the double parallelogram flexure is adopted to remove the parasitic motions. The PEA with a fixed gain of 15 is used to provide excitation voltage for the PCA in the 0–150-V range. To measure the real-time position of the PCA on the nanometer scale, the strain gauge sensor (SGS) bonded to the piezoceramic stack actuator is used in this work. Compared with the capacitive sensor and linear variable differential transformer sensor, the SGS is a contact type sensor, which offers high resolution and bandwidth [1], [40]. The output signals of the SGS pass through the SC, which are simultaneously sampled by the 16-b ADC for the dSPACE-DS1103 controller. Fig. 13 shows the block diagram of the experimental platform.

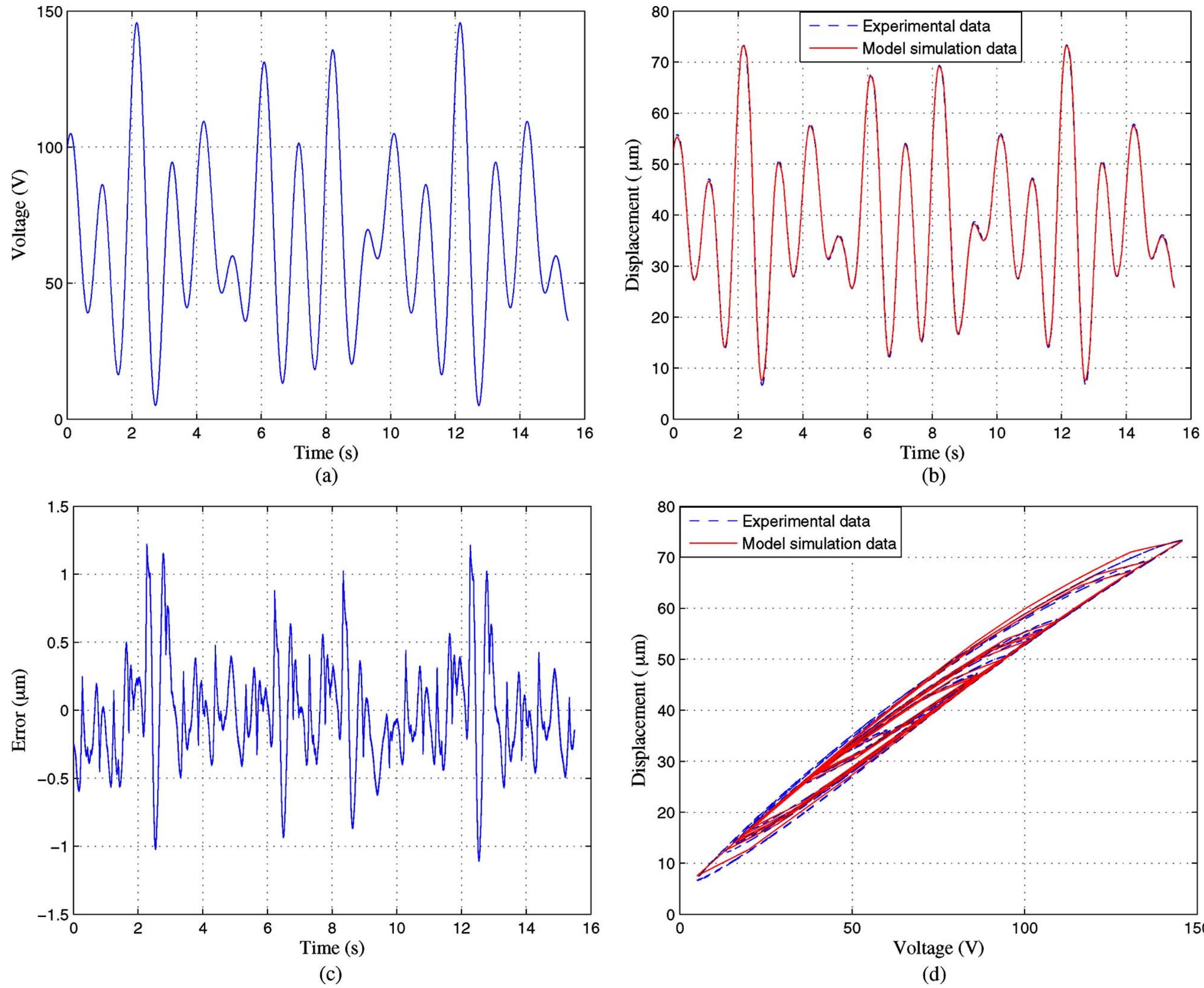

Fig. 16. Experimental verification of the MPI model with a complex input signal. (a) Input voltage. (b) Displacement. (c) Error. (d) Hysteresis loops.

B. Asymmetric Hysteresis Description Results

In practice, the threshold values r_i in the MPI model (7) are given by

$$r_i = \frac{i-1}{n} \left\| v(t) \right\|_\infty , \quad i = 1, 2, \ldots, n \tag{13}$$

with $\|v(t)\|_\infty = 1$ in the normalized case.

To experimentally validate the proposed model, the first step is the identification of the model parameters. Due to the highly nonlinear, high-dimensional, and multiple constraint characteristics, the identification of the hysteresis models is a challenging task, and many identification algorithms have been developed to solve the problem [6], [41]–[43] such as the least square method, genetic algorithms, and particle swarm optimization (PSO). PSO [44] has been shown to be superior to its competitors for the identification of the P-I model. Without losing generality, the PSO algorithm [45] is borrowed in this work to simultaneously obtain the weighted parameters $b(r_i)$, and coefficients a_1, and a_2 of the polynomial input function with the fixed threshold values r_i in (13). Table I lists the identified parameters of the MPI model (7) with ten OSP operators (i.e., $n = 10$). It should be noted that the larger n is selected; it is more precise to describe the hysteresis loops in theory. In real applications, it is verified that further increase of the numbers of the OSP operators leads to no significant improvement in the modeling accuracy. As an illustration, Fig. 14 shows comparisons of identification errors with three different values of n. From this figure, it can be observed that the identification errors are at the same level with the three n's. In the following development, we select $n = 10$ for a case study. To intuitively demonstrate the advantage of fewer parameters in the proposed MPI model, Table II lists a quantified comparison with existing asymmetric P-I models [18], [34]–[36] when the number of threshold n is chosen as 10.

With the identified parameters of the proposed MPI model, Fig. 15 shows the comparison of experimental data of the PCA and associated prediction results of the MPI model. The waveforms of the input voltage, displacement, prediction error, and hysteresis loops are shown in Fig. 15 for the case in which the input voltage is a simple triangle waveform with three dominant maximum values. From Fig. 15(b), it is observed that the prediction results of the MPI model agree well with the experimental measurements. Fig. 15(c) shows that the maximal prediction error is about 1.4% as a percentage of the full displacement range. In addition, the comparison of the hysteresis loops is given in Fig. 15(d). It can be seen that the proposed MPI model well describes the asymmetric hysteresis nonlinearity of the PCA with both major and minor loops.

To further verify the effectiveness of the MPI model, Fig. 16 shows the validation of the MPI model with a complex input signal, where the waveforms of the input voltage, displacement, prediction error, and hysteresis loops are given. From Fig. 16, it is observed that the proposed MPI model presents excellent performance in simulating the complex hysteresis loops. In this case, the maximal error between the prediction and experimental results is about 2.1%, which is slightly larger than the one for the simple input signal. According to the results as shown in Figs. 15 and 16, the mean modeling errors with the MPI model are all less than 1%.

To demonstrate the advantage of the developed MPI model, the CPI model is also adopted to describe the hysteresis nonlinearity of the PCA under the same excitation of the complex input signal shown in Fig. 16(a). The modeling results with the CPI model are shown in Fig. 17. It can be observed that the CPI model can only characterize the symmetric hysteresis and the prediction output of the CPI model is far from the experimental output of the PCA. Therefore, using the CPI model to describe the asymmetric hysteresis in the PCA leads to large errors, which motivates the development of the MPI model in this work to characterize the asymmetric hysteresis nonlinearity. As an illustration, Fig. 18 shows the prediction errors of the CPI and MPI models. It can be seen that the prediction error of the CPI model is three times larger than that of the MPI model. In summary, we can conclude that the proposed MPI model well characterizes the asymmetric hysteresis loops of the PCAs with higher accuracy.

C. Asymmetric Hysteresis Compensation Results

By using the inverse compensator (9)–(12), Fig. 19 demonstrates the inverse hysteresis compensation performance for the PCA with the identified model parameters in Table I. Fig. 19(a) shows a comparison of the desired and actual trajectories, where the actual trajectory well follows the desired trajectory. Fig. 19(b) shows the tracking errors defined as the difference between the desired position and the actual position. It is worthy of mentioning that, due to the existence of modeling uncertainty, the tracking errors exhibit asymmetry about the zero error level. To quantify the performance of the inverse compensator, the root-mean-square error $e_{\rm rms}$ with respect to the full displacement range is calculated by

$$e_{\rm rms} = \frac{\sqrt{\frac{1}{N}\sum_{i=1}^{N}\left(y_{di}-y_i\right)^2}}{\max\limits_i(y_{di}) - \min\limits_i(y_{di})} \times 100\% = 1.3\% \qquad (14)$$

and the maximum error e_m is

$$e_m = \frac{\max\limits_i(y_{di}-y_i)}{\max\limits_i(y_{di}) - \min\limits_i(y_{di})} \times 100\% = 3.7\% \qquad (15)$$

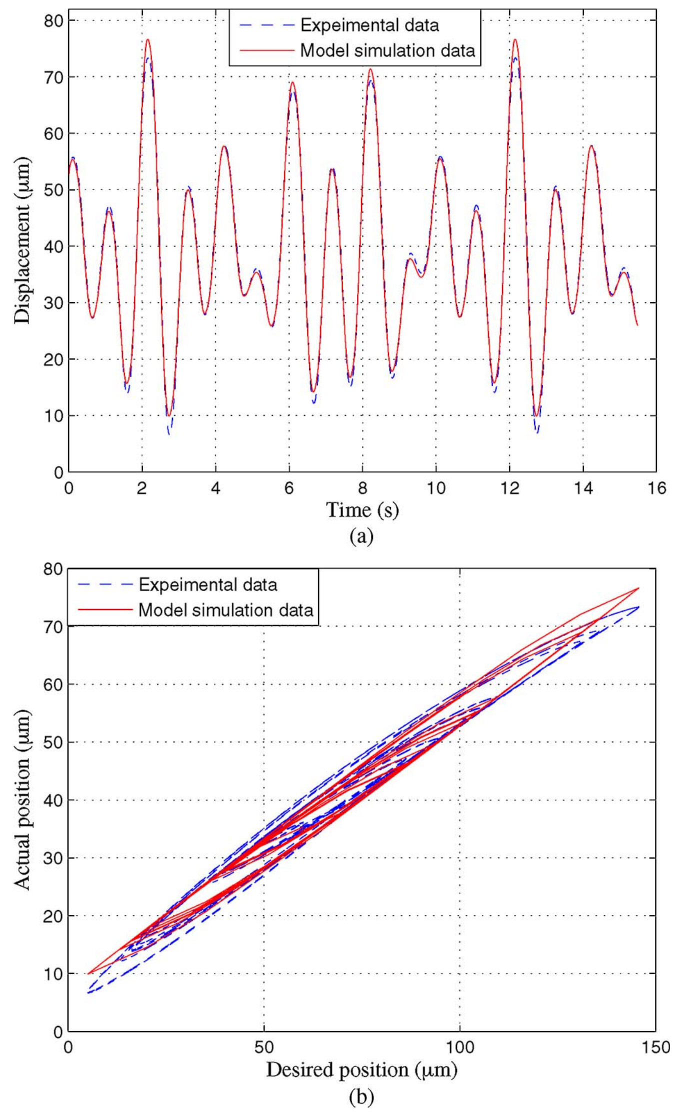

Fig. 17. Experimental verification of the CPI model with a complex input signal. (a) Displacement. (b) Hysteresis loops.

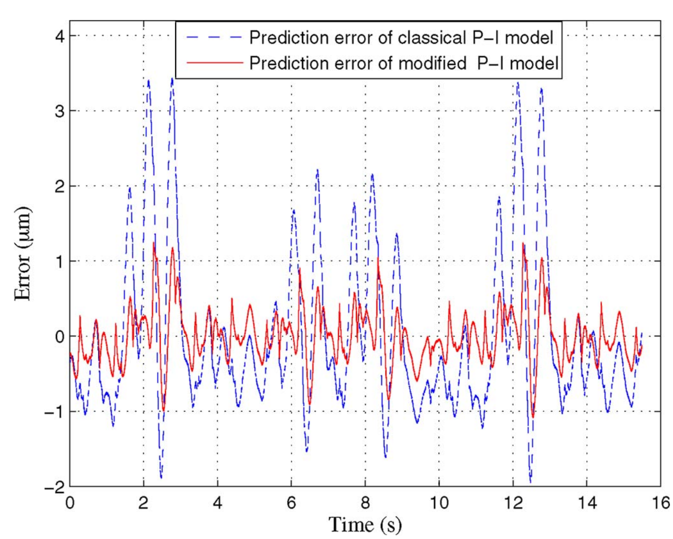

Fig. 18. Comparison of prediction errors with the CPI and MPI models.

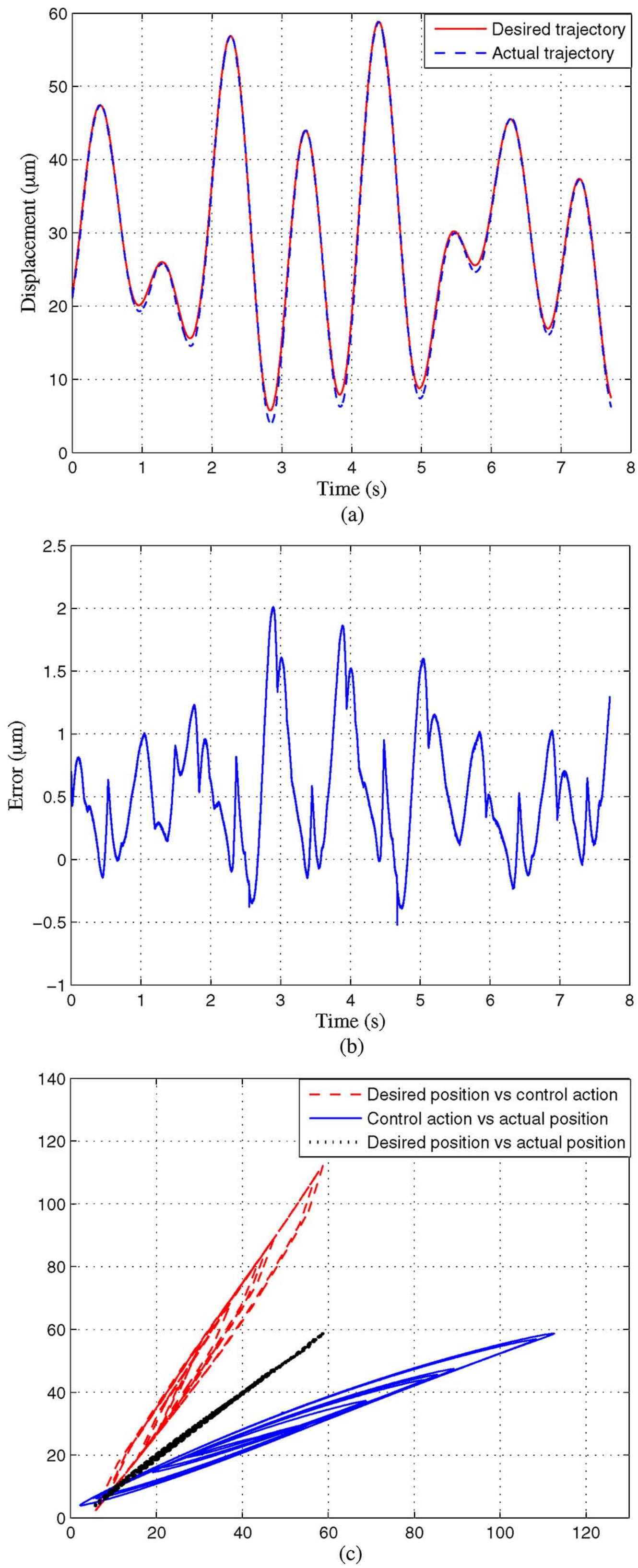

Fig. 19. Demonstration of the inverse hysteresis compensation performance. (a) Trajectory following. (b) Error. (c) Three kinds of input–output relationships.

where N is the number of experimental data points and y_i and y_{di} are the actual and desired positions at the ith data point. Fig. 19(c) illustrates how the inverse hysteresis compensator

TABLE III
TRACKING PERFORMANCE FOR DESIRED SIGNALS
$x_d(t) = \mathrm{A}\sin(2\pi t) + 37.5(\mu\mathrm{m})$

Performance	e_m	e_{rms}
$A = 7.5$	2.93%	1.03%
$A = 15$	2.17%	1.06%
$A = 22.5$	2.59%	1.08%
$A = 30$	2.61%	1.11%

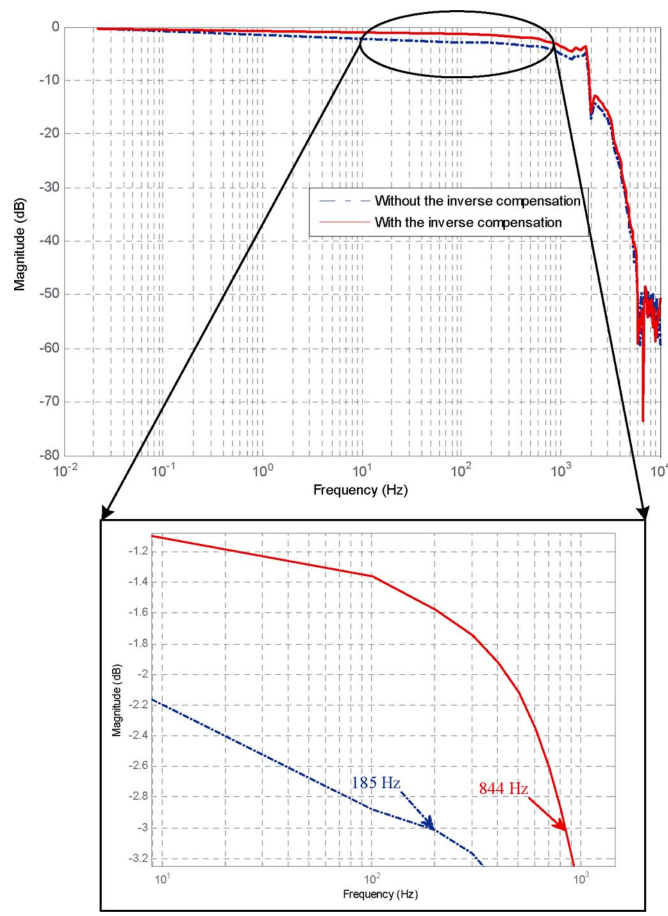

Fig. 20. Amplitude response of the system with and without the inverse hysteresis compensation.

linearizes the asymmetric hysteresis nonlinearity, where both the inverse major-loop and minor-loop hysteresis loops with asymmetric characteristics are produced by the inverse hysteresis compensator to cancel the corresponding real asymmetric hysteresis effect. Furthermore, analyzing the experimental data, the maximum hysteresis-caused error e_m with the inverse compensator is reduced by up to 72.7% compared with the maximum hysteresis-caused error in the open-loop response which is reduced by only 13.6%.

To further verify the inverse compensator with the developed MPI model, experiments with periodic sinusoidal references $x_d(t) = A\sin(2\pi t) + 37.5$ (μm) are conducted. Table III summarizes the tracking performances e_m and e_{rms} at various amplitudes A. It therefore clearly demonstrates the effectiveness of the inverse compensator with the MPI model for the asymmetric hysteresis compensation of the PCA. As a last example, the frequency response of the system with the inverse compensator is studied. Fig. 20 shows the amplitude response of the system with and without the inverse hysteresis compensation. It can be seen that the -3-dB bandwidth is increased from 185 Hz (without the inverse compensation) to 884 Hz (with the inverse compensation).

V. Conclusion

Due to the construction of the analytical inverse, the CPI model is an effective method to describe and compensate for the symmetric hysteresis nonlinearity. Since the CPI model is developed only for describing the symmetric hysteresis, it yields considerable errors for the asymmetric hysteresis. To remedy this drawback, an MPI model was developed in this work to characterize the asymmetric hysteresis nonlinearity of PCAs. The experimental results show that, with the use of MPI, the modeling error is reduced by up to 66.7% compared with the CPI model. Using the MPI model, an analytic inverse hysteresis model can be directly derived from the inverse of the CPI model. Experimental results on a piezoceramic actuated platform were also presented to verify the effectiveness of the developed MPI model and the inverse hysteresis compensator.

In the future, the robust feedback controller, together with the MPI model-based feedforward compensator, will be designed to further improve the tracking performance of the PCAs.

References

[1] S. Devasia, E. Eleftheriou, and S. O. R. Moheimani, "A survey of control issues in nanopositioning," *IEEE Trans. Control Syst. Technol.*, vol. 15, no. 5, pp. 802–823, Sep. 2007.

[2] G.-Y. Gu, L.-M. Zhu, C.-Y. Su, and H. Ding, "Motion control of piezoelectric positioning stages: Modeling, controller design, and experimental evaluation," *IEEE/ASME Trans. Mechatronics*, vol. 18, no. 5, pp. 1459–1471, Oct. 2013.

[3] Y. Li and Q. Xu, "A novel piezoactuated XY stage with parallel, decoupled and stacked flexure structure for micro/nano positioning," *IEEE Trans. Ind. Electron.*, vol. 58, no. 8, pp. 3601–3615, Aug. 2011.

[4] B. J. Kenton and K. K. Leang, "Design and control of a three-axis serial-kinematic high-bandwidth nanopositioner," *IEEE/ASME Trans. Mechatronics*, vol. 17, no. 2, pp. 356–369, Apr. 2012.

[5] X. K. Chen and T. Hisayam, "Adaptive sliding-mode position control for piezo-actuated stage," *IEEE Trans. Ind. Electron.*, vol. 55, no. 11, pp. 3927–3934, Nov. 2008.

[6] K. Kuhnen and P. Krejci, "Compensation of complex hysteresis and creep effects in piezoelectrically actuated systems—A new Preisach modeling approach," *IEEE Trans. Autom. Control*, vol. 54, no. 3, pp. 537–550, Mar. 2009.

[7] H. C. Liaw and B. Shirinzadeh, "Robust adaptive constrained motion tracking control of piezo-actuated flexure-based mechanisms for micro/nano manipulation," *IEEE Trans. Ind. Electron.*, vol. 58, no. 4, pp. 1406–1415, Apr. 2011.

[8] Q. Xu and Y. Li, "Micro-/nanopositioning using model predictive output integral discrete sliding mode control," *IEEE Trans. Ind. Electron.*, vol. 59, no. 2, pp. 1161–1170, Feb. 2012.

[9] Z. Li, "Trilateral tele-operation of adaptive fuzzy force/motion control for nonlinear teleoperators with communication random delays," *IEEE Trans. Fuzzy Syst.*, 2012. [Online]. Available: http://dx.doi.org/10.1109/TFUZZ.2012.2224116

[10] M. Rakotondrabe, C. Clevy, and P. Lutz, "Complete open loop control of hysteretic, creeped, and oscillating piezoelectric cantilevers," *IEEE Trans. Autom. Sci. Eng.*, vol. 7, no. 3, pp. 440–450, Jul. 2010.

[11] K. K. Leang, Q. Zou, and S. Devasia, "Feedforward control of piezoactuators in atomic force microscope systems," *IEEE Control Syst. Mag.*, vol. 29, no. 1, pp. 70–82, Feb. 2009.

[12] D. C. Jiles and D. L. Atherton, "Theory of ferromagnetic hysteresis," *J. Magn. Magn. Mater.*, vol. 61, no. 1/2, pp. 48–60, Sep. 1986.

[13] R. C. Smith, *Smart Material Systems: Model Development*. Philadelphia, PA, USA: SIAM, 2005.

[14] A. Visintin, *Systems With Hysteresis*. New York, NY, USA: Springer-Verlag, 1994.

[15] I. Mayergoyz, *Mathematical Models of Hysteresis and Their Applications*. Amsterdam, The Netherlands: Elsevier, 2003.

[16] P. Krejci, *Hysteresis Convexity and Dissipation in Hyperbolic Equations*. Tokyo, Japan: Gakkotosho, 1996.

[17] M. Rakotondrabe, Y. Haddab, and P. Lutz, "Quadrilateral modeling and robust control of a nonlinear piezoelectric cantilever," *IEEE Trans. Control Syst. Technol.*, vol. 17, no. 3, pp. 528–539, May 2009.

[18] M. Al Janaideh, S. Rakheja, and C. Y. Su, "A generalized Prandtl-Ishlinskii model for characterizing the hysteresis and saturation nonlinearities of smart actuators," *Smart Mater. Struct.*, vol. 18, no. 4, pp. 045001-1–045001-9, Apr. 2009.

[19] G. Aguirre, T. Janssens, H. V. Brussel, and F. Al-Bender, "Asymmetric-hysteresis compensation in piezoelectric actuators," *Mech. Syst. Signal Process.*, vol. 30, pp. 218–231, Jul. 2012.

[20] B. A. Gozen and O. B. Ozdoganlar, "A method for open-loop control of dynamic motions of piezo-stack actuators," *Sens. Actuators A, Phys.*, vol. 184, pp. 160–172, Sep. 2012.

[21] Q. Xu, "Identification and compensation of piezoelectric hysteresis without modeling hysteresis inverse," *IEEE Trans. Ind. Electron.*, vol. 60, no. 9, pp. 3927–3937, Sep. 2013.

[22] S. Rosenbaum, M. Ruderman, T. Strohla, and T. Bertram, "Use of Jiles-Atherton and Preisach hysteresis models for inverse feed-forward control," *IEEE Trans. Magn.*, vol. 46, no. 12, pp. 3984–3989, Dec. 2010.

[23] C. Visone, "Hysteresis modelling and compensation for smart sensors and actuators," *J. Phys., Conf. Ser.*, vol. 138, no. 1, p. 012028, 2008.

[24] P. Ge and M. Jouaneh, "Tracking control of a piezoceramic actuator," *IEEE Trans. Control Syst. Technol.*, vol. 4, no. 3, pp. 209–216, May 1996.

[25] H. Hu and R. B. Mrad, "On the classical Preisach model for hysteresis in piezoceramic actuator," *Mechatronics*, vol. 13, no. 2, pp. 85–94, Mar. 2002.

[26] G. Song, J. Q. Zhao, X. Q. Zhou, and J. A. de Abreu-Garcia, "Tracking control of a piezoceramic actuator with hysteresis compensation using inverse Preisach model," *IEEE/ASME Trans. Mechatronics*, vol. 10, no. 2, pp. 198–209, Apr. 2005.

[27] R. Iyer and X. Tan, "Control of hysteretic systems through inverse compensation," *IEEE Control Syst. Mag.*, vol. 29, no. 1, pp. 83–99, Feb. 2009.

[28] M. Brokate and J. Sprekels, *Hysteresis and Phase Transitions*. New York, NY, USA: Springer-Verlag, 1996.

[29] H. Janocha and K. Kuhnen, "Real-time compensation of hysteresis and creep in piezoelectric actuators," *Sens. Actuators A, Phys.*, vol. 79, no. 2, pp. 83–89, Feb. 2000.

[30] P. Krejci and K. Kuhnen, "Inverse control of systems with hysteresis and creep," *Proc. Inst. Elect. Eng—Control Theory Appl.*, vol. 148, no. 3, pp. 185–192, May 2001.

[31] J. Fu, W. F. Xie, and S. P. Wang, "Robust adaptive control of a class of nonlinear systems with unknown Prandtl-Ishilinskii-like hysteresis," in *Proc. Joint 48th IEEE Conf. Decision Control/28th Chinese Control Conf.*, 2009, pp. 2448–2453.

[32] M. Al Janaideh, S. Rakheja, and C. Y. Su, "An analytical generalized Prandtl-Ishlinskii model inversion for hysteresis compensation in micropositioning control," *IEEE/ASME Trans. Mechatronics*, vol. 16, no. 4, pp. 734–744, Aug. 2011.

[33] Y. Shan and K. K. Leang, "Dual-stage repetitive control with Prandtl-Ishlinskii hysteresis inversion for piezo-based nanopositioning," *Mechatronics*, vol. 22, no. 3, pp. 271–281, Apr. 2012.

[34] K. Kuhnen, "Modeling, identification and compensation of complex hysteretic nonlinearities: A modified Prandtl-Ishlinskii approach," *Eur. J. Control*, vol. 9, no. 4, pp. 407–418, 2003.

[35] R. Dong and Y. Tan, "A modified Prandtl-Ishlinskii modeling method for hysteresis," *Phys. B*, vol. 404, no. 8–11, pp. 1336–1342, May 2009.

[36] H. Jiang, H. Ji, J. Qiu, and Y. Chen, "A modified Prandtl-Ishlinskii model for modeling asymmetric hysteresis of piezoelectric actuators," *IEEE Trans. Ultrason., Ferroelectr., Freq. Control*, vol. 57, no. 5, pp. 1200–1210, May 2010.

[37] C. H. Ru and L. N. Sun, "Improving positioning accuracy of piezoelectric actuators by feedforward hysteresis compensation based on a new mathematical model," *Rev. Sci. Instrum.*, vol. 76, no. 9, pp. 095111-1–095111-8, Sep. 2005.

[38] S. Bashash and N. Jalili, "A polynomial-based linear mapping strategy for feedforward compensation of hysteresis in piezoelectric actuators," *J. Dyn. Syst., Meas. Control*, vol. 130, no. 3, pp. 1–10, Apr. 2008.

[39] S. Liu and C. Y. Su, "A note on the properties of a generalized Prandtl-Ishlinskii model," *Smart Mater. Struct.*, vol. 20, no. 8, pp. 087003-1–087003-7, Aug. 2011.

[40] W. O'Brien, "Piezoresistive sensors: Facilitate high-speed nanopositioning," *Photon. Spectra*, vol. 37, no. 7, pp. 90–92, 2003.

[41] L. Liu, K. K. Tan, C. S. Teo, S. Chen, and T. H. Lee, "Development of an approach toward comprehensive identification of hysteretic dynamics in piezoelectric actuators," *IEEE Trans. Control Syst. Technol.*, 2012. [Online]. Available: http://dx.doi.org/10.1109/TCST.2012.2200896

[42] C. Chan and G. Liu, "Hysteresis identification and compensation using a genetic algorithm with adaptive search space," *Mechatronics*, vol. 17, no. 7, pp. 391–402, Sep. 2007.

[43] Z. Li and C. Yang, "Neural-adaptive output control of a class of transportation vehicles based on wheeled inverted pendulum models," *IEEE Trans. Control Syst. Technol.*, vol. 20, no. 6, pp. 1583–1591, Nov. 2012.

[44] M. J. Yang, G. Y. Gu, and L. M. Zhu, "Parameter identification of the generalized Prandtl-Ishlinskii model for piezoelectric actuators using modified particle swarm optimization," *Sens. Actuators A, Phys.*, vol. 189, pp. 254–265, Jan. 2013.

[45] Q. Li, W. Chen, Y. Wang, S. Liu, and J. Jia, "Parameter identification for PEM fuel-cell mechanism model based on effective informed adaptive particle swarm optimization," *IEEE Trans. Ind. Electron.*, vol. 58, no. 6, pp. 2410–2419, Jun. 2011.

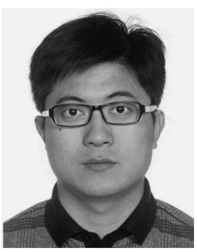

Guo-Ying Gu (S'10–M'13) received the B.E. degree in electronic engineering and the Ph.D. degree in mechanical engineering from Shanghai Jiao Tong University, Shanghai, China, in 2006 and 2012, respectively.

He is currently a Postdoctoral Research Fellow with the School of Mechanical and Power Engineering, Shanghai Jiao Tong University. He was a Visiting Researcher with Concordia University, Montreal, QC, Canada (from October 2010 to March 2011 and from November 2011 to March 2012). His research interests include motion control of nanopositioning stages for scanning probe microscopy applications, robust control, modeling, and control of smart material-based actuators with hysteresis.

Dr. Gu was the recipient of the Scholarship Award for Excellent Doctoral Student granted by the Ministry of Education of China in 2011 and the Best Conference Paper Award at the 2011 IEEE International Conference on Information and Automation.

Li-Min Zhu (M'12) received the B.E. (with honors) and Ph.D. degrees in mechanical engineering from Southeast University, Nanjing, China, in 1994 and 1999, respectively.

From November 1999 to January 2002, he was a Postdoctoral Fellow with Huazhong University of Science and Technology, Wuhan, China. In March 2002, he was appointed Associate Professor in the Robotics Institute, Shanghai Jiao Tong University, Nanjing. Since August 2005, he has been a Professor. He was a Visiting Scholar with Monash University, Clayton, Australia (from September 1997 to May 1998) and the City University of Hong Kong, Kowloon, Hong Kong (from December 2000 to March 2001). His research interests include CNC machining and optical inspection of complex shaped parts and control, sensing, and instrumentation for micro-/nanomanufacturing.

Chun-Yi Su (SM'98) received the Ph.D. degree from South China University of Technology, Guangzhou, China, in 1990.

He is currently with the College of Automation Science and Engineering, South China University of Technology, on leave from Concordia University, Montreal, QC, Canada. Prior to joining Concordia University in 1998, he was with the University of Victoria, Saanich, BC, Canada, from 1991 to 1998. He conducts research in the application of automatic control theory to mechanical systems. He is particularly interested in the control of systems involving hysteresis nonlinearities. He is the author or coauthor of over 300 publications that appeared in journals, as book chapters, and in conference proceedings.

Dr. Su has served as an Associate Editor of the IEEE TRANSACTIONS ON AUTOMATIC CONTROL, IEEE TRANSACTIONS ON CONTROL SYSTEMS TECHNOLOGY, and *Journal of Control Theory and Applications*. He is on the Editorial Board of 14 journals, including the IFAC journals *Control Engineering Practice* and *Mechatronics*. He has also served many conferences as an organizing committee member, including General Cochair of the 2012 IEEE International Conference on Mechatronics and Automation and Program Chair of the 2007 IEEE Conference on Control Applications.